Eocene ultra high temperature (UHT) metamorphism in the Gruf complex (Central Alps): constraints by LA-ICPMS zircon and monazite dating in petrographic context.

Christian Nicollet, Valérie Bosse, Maria Iole Spalla

Eocene ultra high temperature (UHT) metamorphism in the Gruf complex (Central Alps): constraints by LA-ICPMS zircon and monazite dating in petrographic context.

Christian Nicollet[1*], Valérie Bosse[1] & Maria Iole Spalla[2]

[1]*Laboratoire Magmas et Volcans, Université Clermont Auvergne, CNRS, IRD, OPGC, F-63000 Clermont-Ferrand, France*

[2]*Dipartimento di Scienze della Terra "A. Desio", Università degli Studi di Milano, Via Mangiagalli 34, 20133 Milano, Italia.*

**Corresponding author (e-mail:Christian.nicollet@uca.fr)*

The Gruf complex in the Lepontine Alps is one of the rare occurrences of Phanerozoic UHT metamorphism in the world but its age is still a matter of debate. Here we present LA-ICPMS dating in petrographic context of zircon and monazite from an UHT restitic granulite. Zircons and monazites are both included in large crystals and in retrograde symplectites. In such restitic rocks, partial melting or fluid interactions are unlikely precluding resetting of the monazite chronometers. Zircon cores yield Permian ages interpreted as age of charnockitisation. They are sometimes surrounded by a narrow rim at 32 Ma. Monazites are strongly zoned, but all yield a 31.8 ± 0.3 Ma age interpreted as the time of complete (re-)crystallisation during the UHT paragenesis. We propose that the zircons dated a post Hercynian metamorphism which is responsible of the widespread formation of granulites in the Southern Alps and the crust differentiation. This fluid-absent melting event produced refractory lithologies such as restites in charnockites. We suggest that Gruf UHT paragenesis is alpine in age and cristallised from these refractory lithologies. We conclude that the lower restitic crust produced at the Permian time had the ability to achieve UHT conditions during the fast exhumation and heating related to lithospheric thinning in Alpine time.

Supplementary material: Analytical procedures for monazite analysis and dating; table of major elements of the minerals; table of the isotope data.

Introduction

The Gruf complex in the Lepontine Alps is one of the rare occurrences of Phanerozoic UHT metamorphism in the world, discovered in the Val Codera by Cornelius (1916), Cornelius & Dittler (1929), and described by Barker (1964), Wenk et al. (1974). Because occurrences of UHT metamorphism are mainly of Precambrian age (eg Harley, 1998; Brown, 2007; Kelsey and Hand, 2015), this area is of major interest to understand the geodynamic signification of such extreme metamorphic conditions. Indeed, the main difficulty in understanding the geodynamic significance of UHT metamorphism is that Precambrian UHT granulites are often preserved in small-scale

lenses: they usually represent structural and metamorphic relics in polymetamorphic rocks belonging to polycyclic terrains. The lack of large-scale tectonic structures associated to their emplacement precludes a clear understanding of their geodynamic history. Thereby the few Phanerozoic UHT occurrences for which the geological context is well constrained are precious records that help to understand and interpret this type of metamorphism.

The age of the UHT metamorphism in the Gruf complex is currently a matter of debate. Based on zircon U/Pb dating, Galli et al. (2012) have proposed a Permian age (282 – 260 Ma) for the granulite facies fluid-absent biotite melting event. For these authors, the presence of orthopyroxene inclusions in zircons confirms the Permian age of the charnockites and associated sapphirine-bearing granulites. Zircon rims from the same samples yield 34-29 Ma ages interpreted as dating the Alpine amphibolite facies migmatisation. A different interpretation was suggested by Droop and Bucher (1984) and proposed by Liati and Gebauer (2003). The latter authors considered that the zircon Alpine rims (yielding a weighted mean age at 32.7 ± 0.5 Ma in their samples) grew during the UHT metamorphic event, and that the sapphirine-bearing granulites were restites formed during partial melting of the Permian granitoids. Moreover, Schmitz et al. (2009) measuring an age of 33.0 ± 4.4 by monazite chemical dating also agree with this interpretation.

These contrasting results imply two different models for the origin of the UHT metamorphism: 1) a Permian UHT metamorphism can be linked to the post Hercynian high-thermal regime, associated with lithospheric Permian-Triassic thinning and responsible for of the widespread formation of granulites in the Austroalpine and South -Alpine continental crust (e.g.: Broadie et al., 1989; Lardeaux and Spalla, 1991; Diella et al., 1992; Barboza and Bergantz, 2000; Muntener et al. 2000; Schuster et al., 2001; Spalla and Marotta, 2007; Schuster and Stuewe 2008; Galli et al., 2013; Spalla et al., 2014). This anomalously high thermal regime would be responsible for a pervasive melting event, associated with melt loss leading to the genesis of a residual, refractory lower crust. Such processes are interpreted to be responsible of the lower continental crust differentiation (e.g. Vielzeuf and Holloway, 1988; Brown, 2008; Redler et al., 2013); 2) An Alpine UHT metamorphism would have been driven by lithospheric thinning associated with slab breakoff and asthenospheric upwelling ((e.g. Davies and von Blanckenburg, 1995; von Blanckenburg and Davies, 1995; Oalman et al., 2016) which would provide the considerable amount of heat necessary to reach the UHT conditions.

In this study, we combine for the first time zircon and monazite in situ dating in petrographic context for the Gruf sapphirine granulite. The results provide a new opportunity to clarify the age of the UHT event and its geodynamic context.

Geological setting

Penninic nappes in the Central Alps consist of variegated rocks of continental and oceanic origins. This nappe stack is separated from the Southern Alps by the Periadriatic Lineament and by a thin ribbon of Austroalpine crust verticalised along the "southern steep belt" (e.g. Schmid et al., 1996). The axial portion of Central Alps has recorded a polycyclic metamorphic evolution: structural and petrologic relics of Hercynian and Caledonian imprints have been described (Schaltegger, 1994; Spalla et al., 2014 and refs therein). The Alpine overprint occurs with heterogeneous intensity, and the separation of Alpine from pre-Alpine metamorphic imprints has remained for a long time difficult due to the similar metamorphic conditions associated with these successive orogenic cycles (e.g.: Niggli, 1974; Engi et al., 2004). Alpine metamorphism in the Central Alps is characterized by a polyphasic metamorphic evolution characterised by an early high pressure- low- to intermediate-temperature imprint, preserved as relic blueschist- and eclogite-facies assemblages, recorded during the south-verging subduction. The second metamorphic imprint is characterised by assemblages indicating a Barrow-type event interpreted as consequent to the continental collision. Isograds of the Barrovian metamorphism define the "Lepontine metamorphic dome" (Trommsdorff, 1966; Todd and Engi, 1997) and their concentric distribution indicates that metamorphic conditions increase southwards from greenschists- to upper amphibolite-facies. In this southern part migmatisation conditions have been attained at about 700°C and 0.6-0.8 GPa between 32 and 22 Ma (Engi et al., 1995; Burri et al, 2005; Berger et al, 2009; Rubatto et al., 2009). The Gruf complex (Fig. 1) is a small tectonic unit of about 200 km^2, located in the southeastern part of the Lepontine dome, north of the Insubric Line, and limited to the east by the calc-alkaline Tertiary intrusive stock of Bergell. This intrusive massif is considered synchronous with crustal anatexis at 33 - 28 Ma (Berger et al. 1996). The Gruf complex is composed mainly of biotite-garnet-sillimanite-cordierite metapelitic rocks and migmatitic orthogneisses and paragneisses, and has been recently considered as part of the tectonic mélange of continental and oceanic units accreted together in the Alpine tectonic accretion channel (Engi et al., 2001). During a remarkable field work in a very difficult terrain Galli et al. (2012) described structural and petrologic characters of the complex in situ for the first time, focusing especially the Mg-Al-rich sapphirine granulites. The latter form schlieren and residual enclaves within sheet like bodies of charnockites and migmatitic orthogneisses (Galli et al., 2013). The chemical composition of the Mg-Al-rich granulites is comparable to that of restitic surmicaceous enclaves in granites (e.g. Montel et al., 1991) except for magnesium. Kelsey et al. (2003) suggested that the production of Mg-Al-rich compositions through melt loss is improbable because of the low Mg partition into melt. For these authors Mg-rich assemblages may source from Mg-enriched protoliths. Consequently, the Gruf Mg-Al-rich sapphirine granulites may represent resister lenses within charnockites/orthogneisses or restites from Mg-rich protolith included in the

charnockites.

Previous published geochronological studies are at the origin of the contrasted interpretations for the geodynamic signification of the UHT conditions recorded in the Gruf complex. Liati and Gebauer (2003) report SHRIMP weighted mean ages at 272.0 ± 4.1 Ma in zircon cores and at 32.7 ± 0.5 Ma in zircon rims from a saphirine bearing granulite sample. The Permian ages are interpreted as reflecting the age of the magmatic protolith whereas the Alpine ages are considered to represent the age of the granulite facies metamorphism. For these authors, sapphirine-bearing granulites represent restites formed during Alpine partial melting of Permian granitoids. Galli et al. (2011; 2012) proposed different interpretation based on similar geochronological data obtained with the same method (Zircon SHRIMP analyses). For these authors 282-260 Ma ages obtained in oscillatory zoned zircon cores represent melts generated through granulite facies fluid-absent biotite melting at 920-940°C in metapelitic rocks, whereas 34-29 Ma ages in zircon rims date the Alpine amphibolite facies migmatisation. For these authors the charnockites associated with the sapphirine-bearing granulites belong to the post-Hercynian European lower crust. Schmitz et al. (2009) applied the method of 3D-Micro X-ray fluorescence analysis on monazite in thin section from a sapphirine-bearing granulite. They obtained an age at 33.0 ± 4.4 Ma in monazites included in and intergrown with HT minerals which they interpreted as the age of the high-temperature event. Finally, Oalmann et al. (2013, 2016) also suggest that UHT conditions were reached slightly before 32.5 Ma followed by cooling from 30 to 19 Ma recorded by rutile $^{206}Pb/^{238}U$ ages.

Petrography of the Mg-Al granulites

Mg-Al-rich sapphirine granulites have been already carefully described by Barker (1964), Droop and Bucher (1984), Galli et al., (2011) and Guevara and Caddick (2016). We will concentrate here on the main petrological characters and mineral reactions, which appear to be of major interest to link petrology and geochronology. The studied sample is a pebble which has been collected in upper Val Codera (Fig. 1). Two domains have been recognized at the sample scale: one is a sapphirine-bearing granulite (Fig. 2a) while the other has the typical mineralogy of a charnockite (Figs. 2d and e). The boundary between these two domains is progressive. Following Galli et al (2011), we admit that the granulitic domain could be a restite/schlieren of Mg-rich metapelite or perhaps a resister within the charnockitic domain. The charnockitic paragenesis is composed of millimetric to pluri-millimetric crystals of Opx - Bt - Kfs ± Pl - Qz - Mnz - Zrn and Ap (Figs. 2d and e). Rare inclusions of zircon, monazite, plagioclase and quartz are observed in the phenocrysts. In some places, clusters of K-feldspar - quartz-apatite microcrysts are following the grain boundaries in the charnockitic assemblage (Fig. 2e). They seem to represent incipient melting or residual melt after extraction. In

the charnockite domain, K-feldspar is orthose (XOr: 80%; XAb: 20%), plagioclase has an intermediate composition with XAn: 40. The compositions of orthopyroxene and biotite are substantially the same as in the granulitic domain of the rock.

The primary crystals of the residual/resister granulite are millimetric to plurimillimetric. The peak UHT paragenesis was: Al rich-Opx - Sil - Spr - Bt - Grt – Crd – Rt – Ap – Zrn - Mnz (Fig. 2a). Here again some tiny inclusions are rarely present. Detailed observations of the mineral associations reveal complex relationships with (at least) 2 generations of Al-rich orthopyroxene, sillimanite, cordierite and sapphirine ± spinel ± biotite, garnet and rare inclusions of quartz, rutile and apatite. Secondary minerals are abundant. Except for orthopyroxene, the chemical composition of the minerals does not change much and the crystals are weakly zoned (Table A supplementary material). Garnet is almost pure almandine – pyrope solid solution with a slight decrease of pyrope relative to almandine at the rim of the crystals (from the core to the rim: XPy: 48-46 %; XAlm: 42-45 %). Grossular and spessartine contents are low: XGrs: 2.2-3.1% and XSp: ≤1%. Opx is Al_2O_3-rich and zoned (core: 7.5-8.6% and rim: 5.5 to 7 % Fig. 3). Biotite is Mg- (XMg: 75-80%) and Ti-rich (TiO2: 2.6-3.6%). Cordierite composition is homogeneous both in primary minerals and in symplectites. Galli et al. (2011), Oalmann et al. (2013), Guevara and Caddick (2016) estimated the conditions of the primary paragenesis in these granulites at T = 920-940 °C and P= 0.85-0.95 GPa.

The secondary symplectites in the granulites are varied and complex, with Spr, Sil, Crd, Opx ± Sp. Spinel is hercynite - spinel solution, homogeneous in composition. Two main reactions dominate (Fig. 2b-c): Sil 1 phenocrysts are surrounded by Spr 2 + Crd 2 in contact with Opx ± Bt; the garnet is destabilized into symplectites of Opx 2 + Crd 2. These two reactions indicate a pressure decrease. Al_2O_3 content in Opx 2 is between 7.4 to 5.9 % similar to the rims of the primary phenocrysts (Fig. 3) whereas the XMg is slightly lower than in the primary crystals. Primary Opx probably continues to grow at the beginning of the retrograde evolution during decompression, while garnet is destabilized. This suggests that primary paragenesis and retrograde symplectites are the product of a single metamorphic event. These retrograde textures demonstrate a re-equilibration of the UHT peak assemblages at lower metamorphic conditions: 720-740 °C at 6.5-7.5 kbar which starts with a decompression and continue with a temperature decrease (Galli et al. 2011; Oalmann et al. 2013; Guevara and Caddick, 2016). These conditions are similar to those inferred for the migmatisation occurring during for the Tertiary Barrovian regional metamorphism (Burri et al, 2005; Engi et al., 1995).

Both zircons and monazites are included in the large crystals from the UHT assemblage as well as in the late symplectites.

Zircon and monazites textures

Zircons are subhedral elongated and/or resorbed rounded crystals 30-100 µm long. They contain rare and very tiny inclusions among which biotite, white mica and apatite were only unequivocally identified by Raman spectrometry. Sillimanite has not been observed. Zircons included in the primary phenocrysts are resorbed grains and seem to be relictual (Fig. 4a). Cathodoluminescence images (CLI) show that most of the grains display a large inner domain with usually oscillatory or rarely complex zoning (Fig. 4b - c). In zircon included in the cordierite or biotite, this inner domain is sometimes surrounded by a thin rim (<5 µm to 15 µm) with euhedral faces and bright in CDI (Fig. 4c). U and Th contents are variable (150<U< ~4860 ppm and 4 <Th<1180 ppm; Table B supplementary material) with no correlation with the internal structure nor ages (see the next section). As a result, Th/U ratios are also variable (0<Th/U<0.50) and not related to the different zircon domains (i.e. oscillatory zoned inner domain or external rim).

Monazites are 50 to 150 µm in size and are present in the core of large Spr, Opx, Crd crystals or form clusters of small grains (10 to 40 µm) in the late symplectites. The shape of the grains varies from large rounded grains to small elongated ones with rarely indented grain boundaries (Fig 5b and 6a), without any correlation with the textural position. Rare inclusions are needles of sillimanite (Fig. 6a). All the grains are strongly zoned (Table 1). Chemical variations of the LREE-, Th- and Ca-contents broadly follow the brabantite substitution ($2REE^{3+} = Th^{4+} + Ca^{2+}$). ThO2 content varies from 1.3 to 10.8 wt%. Y_2O_3 and UO_2 contents are highly variable (from 0.1 to 5.5 wt% and from 0.2 to 3.5 wt%, respectively) and inversely correlated. These variations are clearly related to the zonation of the sample (Fig. 7a): monazites in the charnockite domain are Y-rich and U-poor whereas the opposite is true in the granulite domain. Variations in LREE, MREE and Y_2O_3 contents are also correlated to the sample zonation: monazites from the charnockite domain are enriched in Gd_2O_3 and Y_2O_3 whereas monazites from the granulite domain are enriched in La_2O_3 and poor in Gd_2O_3 and Y_2O_3 (Fig. 7 b - c). Chemical variations are observed from grain to another but also within single crystal (Fig. 6 a - b). Some of the grains display very tiny Y-rich overgrowths (Fig. 6a).

U-Th-Pb geochronology

Monazite and zircon have been analysed in thin section by LA-ICPMS in order to control the position of the grain (and thus the measured ages) relative to the textures observed in the sample. Zircons and monazites were ablated using a Resonetics Resolution M-50 equipped with a 193 nm Excimer laser system coupled to an Agilent 7500 cs ICP-MS with a 1 Hz repetition rate, a fluence of 7 J/cm² and a spot size of 7 µm for monazite dating and 3 Hz repetition rate, a fluence of 2.6 J/cm^2 and a spot size of 20 µm for zircon dating. Helium carrier gas was supplemented with N2

prior to mixing with Ar for sensitivity enhancement (Paquette et al., 2014). Detailed analytical procedures are reported in Paquette and Tiepolo (2007) and Didier et al. (2015) and in Supplementary – Analytical procedures. Monazite can be dated using both U-Pb and Th-Pb decay schemes. Here we will only consider $^{208}Pb/^{232}Th$ ages for the following reasons. Firstly, ^{232}Th is largely predominant in monazite, allowing small spots (7 µm) to be performed during laser ablation. Secondly, U decay series could be in disequilibrium in young monazites (Schärer, 1984), resulting in overestimated $^{206}Pb/^{238}U$ ages. Because secular equilibrium among the intermediate daughters of ^{232}Th occurs after about 30 years, it seems reasonable to assume that initial ^{208}Pb is absent. Thirdly, ^{232}Th is so abundant that ^{208}Pb originating from common Pb is usually negligible compared to radiogenic ^{208}Pb. To reinforce this hypothesis, we only consider here the concordant $^{208}Pb/^{232}Th$ – $^{206}Pb/^{238}U$ ages (Fig. 8a). Whatever the textural position of the monazite grains or the chemical composition of the monazite domain, the $^{208}Pb/^{232}Th$ ages are between 29.6 ± 1.0 and 34.1 ± 1.1 Ma, allowing to calculate a weighted average age of 31.8 ± 0.3 Ma (MSWD = 3,2, N = 51; Fig. 8b; Supplementary material: Table B).

$^{206}Pb/^{238}U$ ages measured in zircon from our sample are scattered from 30 ± 1 to 304 ± 12 Ma (only U/Pb concordant ages; Fig. 8c). The youngest ages have been obtained in the bright rims. Plotted in a Tera Wasserburg diagram, we see that these ages are in total agreement with the ages measured in the monazite grains (Fig. 8c). The oldest ages are upper Carboniferous-lower Permian and have been obtained in the inner oscillatory zoned domains. Two reasons can be provided to explain intermediate ages between the oldest and the youngest ones: i) they reflect mixing between the Carboniferous core and the narrow Cenozoic rim (<5 µm to 15 µm) due to analysis of distinct adjacent domains; ii) they result from Pb loss. Indeed, in some of the grains the U content is high (U> 1000 ppm). Such a high U content could be responsible for radiation damage of the crystal lattice especially in Paleozoic zircons and induce Pb loss. This results in younger core compared to the rim as observed in Figure 4b. With the aim of limiting these two effects and to better restrict the range of the oldest ages, we decide to only consider the ages which were measured i) in the zircon crystals which do not present the luminescent rim on the CLI, ii) measured in domains with U content ≤1000 ppm. By doing this the scattering of the $^{206}Pb/^{238}U$ ages remains between 247 ± 6 and 304 ± 12 Ma (Fig. 8d).

Discussion

- Ages recorded in zircon

Two groups of ages have been recorded in the zircons: between 247 ± 6 and 304 ± 12 Ma in the core and ca 30 Ma in the rim. These ages are in total agreement with the results obtained by Liati

and Gebauer (2003) and Galli et al. (2012). Following these last authors, who found the charnockitic paragenesis included within the zircon cores, the ages measured in the oscillatory zoned inner domain could be interpreted as the age of the charnockitisation. As no older inherited domains have been observed in our zircons, we favour this interpretation. This charnockitisation can be developed under the Permian-Triassic high-thermal regime (Galli et al., 2013) responsible of the widespread formation of granulites in the Southern Alps and Austroalpine (Bertotti et al., 1993; Spalla and Marotta, 2007; Spalla et al., 2014 and references herein). The scattering of the ages between 247 to 304 Ma in a single sample is rather surprising and, as previously suggested, can not be only attributed to mixing ages. Such a large spread of zircon ages is known in other Austroalpine and Southalpine units (Marotta et al., 2016 and refs therein) representing lower continental crust: Ivrea zone (Vavra and Schaltegger, 1999; Peressini et al., 2007), Malenco (Müntener et al., 2000), Sondalo (Tribuzio et al., 1999), Valtournanche (Manzotti et al, 2012). Vavra and Schaltegger (1999) suggest that the U-Pb system in zircons from the Ivrea Zone could have been disturbed by different types of alteration and Pb-loss processes during the Permian, Triassic and possibly early Jurassic times. These perturbations were differently interpreted as consequent to the early stages of Mesozoic rifting related to thermal and/or decompression pulses during extensional unroofing in the Permian (Marotta et al., 2009), as for example in Valtournenche, where the pre-Alpine evolution is associated with LP-HT metamorphism related to Permian-Triassic lithospheric thinning (Manzotti et al, 2012; Manzotti & Zucali, 2013). Our results, although slightly older than the previously published ages (but within 2 σ error bar), are in agreement with these interpretations.

The second group of ages between 30 ± 1 Ma and 34 ± 2 Ma has been recorded in euhedral rims from some of the matrix zircons. Most of the zircons included in the primary phenocrysts do not present such a younger rim (Fig 4 b). Furthermore, these results are similar to the $^{208}Pb/^{232}Th$ ages measured in the adjacent monazites, whatever the textural position of the latter. Thus, these results argue for a zircon recrystallisation event at ca. 32 Ma simultaneaous with the crystallisation (or re-crystallisation, see the discussion below) of the monazite grains.

- What do we learn from the monazite ages ?

Contrary to the zircon results, monazites from the studied sample provide narrow age estimation at 31.8 ± 0.3 Ma (between 29.6 ± 1.0 and 34.1 ± 1.1 Ma). The ages are the same in all the different textural positions of the monazite (included in large Spr, Opx or Crd crystals or in the Crd-Bt matrix or as cluster of small grains within secondary symplectites), or the chemical zoning or the granulitic (Fig. 6a) or charnockitic (Fig. 6b) paragenesis. The Y-rich overgrowth observed in some monazite grains which could be related to the garnet destabilisation do not yield younger ages (Fig. 6a).

Similarly, no older ages (i.e. Paleozoic) have been recorded by the monazites. Usually the shape of the monazite grains suggests equilibrium with, on one hand, the large primary crystals recording the peak of the UHT conditions and on the other hand, with the secondary symplectites during the beginning of the retrograde evolution. This demonstrates that the Spr-Opx-Sil UHT paragenesis as well as the retrograde symplectites in the restitic granulites equilibrated at ca. 32 Ma, in agreement with earlier works (Liati and Gebauer, 2003, Schmitz et al., 2009, Droop and Bucher, 1984). The Alpine UHT event is recorded by the monazite and by the zircon rims.

Galli et al. (2011, 2012, 2013) disagree with this interpretation. In their model, the Alpine age recorded in the zircon rims represent the age of the migmatisation of the Gruf lithologies in the upper amphibolite facies conditions. Moreover, they interpreted that the ages recorded at 33.0 ± 4.4 Ma by monazite (Schmitz et al., 2009) are supposedly the result of the monazite resetting during fluid-assisted migmatisation (Galli et al. 2012). We cannot support this interpretation for two reasons. First, many examples exist in the literature that show that monazite is a robust geochronometer able to retain age records during anatectic processes (Paquette et al. 2004; Rubatto et al. 2006; Stepanov et al. 2012; Rubatto et al. 2013; Didier et al. 2014; Didier et al. 2015) or even UHT conditions (Korhonen et al. 2013; Rocha et al. 2017). The main causes of possible disturbance of the Th-U-Pb systems in monazite are dissolution/recrystallisation processes during melt or hydrous fluid interaction (eg: Cherniak et al., 2004; Kelsey et al. 2012). Fluid interaction in the present context is difficult to argue and in any case supposes an external input (see the next point below). Dissolution/recrystallisation processes during melt interaction strongly depend upon the melt composition and its H2O content (Montel, 1986; Rapp and Watson 1986; Spear and Pyle 2002). Monazite solubility is low in meta- or peraluminous melts and thus monazite is able to resist to crustal anatexis. To conclude, if fluid-assisted migmatisation in the amphibolite conditions occurred during the Alpine times following a Permian UHT event, we would expect to measure Permian ages in part of the monazite domains or grains, which is not the case. “Resetting” cannot be an explanation for the absence of Permian age records in monazite in the present conditions.

The second point questions the migmatisation processes in such refractory lithologies. As reported by Galli et al. (2011), Mg-Al granulites occur as restites or schlieren in the charnockites and thus represent highly refractory rocks formed during partial melting processes in the Permian times. Partial melting of such refractory lithologies is improbable as also suggested by McDade and Harley (2001) unless a high amount of fluid is added. It is very unlikely that this fluid-assisted migmatisation event in the amphibolite facies conditions could be responsible for all the textures observed in the UHT granulites. There is no evidence in the retrograde reactions of significative fluid input as argued by Galli et al. (2011). In contrast we propose that all the metamorphic textures

in the Mg-Al granulites correspond to the UHT conditions during the Alpine time, as demonstrated by the age recorded in the monazites equilibrated with the UHT mineral assemblages.

- A model for the evolution of the Gruf granulites and charnockites

Based on the petrological observations and geochronological results obtained in our sample we propose the following model for the time evolution of the Gruf granulites and charnockites. The oldest ages we obtained in the zircons from our UHT granulite sample are between 304 ± 12 Ma and 247 ± 6 Ma. These ages, despite slightly older, are similar to those measured by Galli et al. (2012) and Liati and Gebauer (2003) in the Gruf UHT granulites. Older ages at 513 ± 8 Ma and 453 ± 8 Ma (weighted average ages in magmatic zircon cores) have only been reported in an enclave-rich biotite orthogneiss in the Gruf complex (Galli et al. 2012). Our results suggest that oscillatory zoned zircons from the UHT granulites crystallized in the Permian-Triassic times during a partial melting event. This Paleozoic anatectic event occured under the granulite facies conditions, as shown by the presence of the charnockitic paragenesis included in the zircons cores (Galli et al.2013), inducing the formation of both charnockitic melt and restitic/resister rocks, the precursor of the sapphirine-bearing granulites. Unfortunately, the few tiny inclusions observed in the zircon grains do not allow to precise what was the mineral assemblage in this precursor during the Paleozoic event. We suggest that the precursor of the sapphirine-bearing granulites was a biotite – cordierite rich selvedge probably containing also orthopyroxene and garnet could have been added. Considering the abundance of the monazites in our sample, it is likely that monazites were present during the Permian times. During the Alpine times, UHT metamorphism occurred during a short-lived event (less than 5 Ma) between 30 to 34 Ma recorded by both zircon rims and monazites. UHT metamorphic conditions at 920-940 °C/ 0.85-0.95 GPa (Galli et al., 2011) are responsible for the complete re-crystallization of both the charnockites and the Bt-Cd-Grt(?)-Opx(?)-bearing rocks and enables the development of UHT parageneses appearance: Al rich-Opx - Sil - Spr - Bt - Grt – Crd – Rt – Ap- Zrn - Mnz in the Mg-Al granulite and Opx, Bt, Kfs, ± Pl, Qz, Zrn, Mnz and Ap in the charnockite. In both the charnockites and the Mg-Al granulites, this UHT event is responsible for the partial dissolution of the Paleozoic zircons and the growth of the Alpine rims. Because no Paleozoic ages were found in monazites from our samples (as well as in the previous monazite study, Schmitz et al. 2009), crystallisation processes for the Alpine monazites are more difficult to assess. Two processes can be proposed: crystallisation from a mineral precursor such as allanite or apatite, or complete recrystallisation of an earlier monazite generation, possibly late Carboniferous – Permian in age. We have no textural evidence of allanite nor apatite-monazite relation in our sample suggesting that these minerals participate to the reaction inducing monazite crystallisation. On the other hand we did not observed nor suspected the presence of older domains in the

monazites that we analysed, suggesting the partial recrystallisation from previous monazite. However, the differences in chemical composition, but identical ages, between the monazites of charnockite and granulite domains (Fig. 7) suggest a local equilibrium between monazite and the charnockite versus granulite UHT mineral assemblages during the Alpine times. We thus propose that Alpine monazites result from the complete recrystallisation of an earlier monazite generation, probably of Paleozoic age, during the crystallisation of UHT parageneses.

- Geodynamic implications and the origin of the UHT metamorphism in the central Alps

The oldest ages we obtained in the zircon cores between 304 ± 12 Ma and 247 ± 6 Ma interpreted as the age of the charnockitisation, unknown elsewhere in the Penninic domain of the Central Alps (Galli et al, 2011),), developed during Permian-Triassic high thermal regime responsible for HT-LP metamorphism widespread in the Austroalpine and Southalpine domains (Galli et al., 2013, Barboza and Bergantz, 2000; Lardeaux and Spalla, 1991; Diella et al., 1992; Bertotti et al., 1993; Muntener et al. 2000; Marotta et al., 2016). These granulites are interpreted as residual and refractory rocks following partial melting events and extensive melt loss. This process is responsible for the differentiation of the continental crust via fluid-absent melting reactions involving muscovite and biotite (and amphibole in metabasic rocks) destabilisation. As a consequence, the precursor of the Al-Mg granulites of the Gruf complex acquired its restitic character during this post Hercynian event.

UHT metamorphism occurs at temperatures above the fluid-absent melting in most crustal rocks which is an endothermic process that consumes heat and buffers the temperature (Vielzeuf and Holloway, 1988; Stüwe 1995). Thus partial melting limits heat production avoiding a fertile crust to attain UHT. Nevertheless, UHT conditions are more easily reached in refractory/restitic rocks and develop preferentially in terrains that previously underwent metamorphism and melt loss (Clark et al., 2011; Kelsey and Hand, 2015). The Gruf complex is the sole unit in Penninic Domain of Central Alps recording the Permian-Triassic granulitic metamorphism, which permitted its rocks to reach and record UHT conditions during the Alpine cycle.

Zircon and monazite ages, together with their microstructural relationships with granulite facies minerals, show that the typical UHT paragenesis crystallised at Alpine time during a short-lived event (less than 5 Ma) between 34 to 30 Ma. These results are in agreement with the garnet diffusion modelling proposed by Galli et al. (2011) also suggesting that UHT metamorphism was brief. This UHT metamorphism is contemporaneous with the Bergell tonalite-granodiorite intrusion

373 dated between 33 and 28 Ma (Berger et al. 1996) and the beginning of the anatectic event in the
374 Southern part of the Central Alps at 32 Ma (Köppel et al, 1981; Berger et al, 2009; Rubatto et al.,
375 2009). Secondary symplectites in the Mg-Al granulites just following the UHT peak conditions are
376 equilibrated in the same conditions as the Lepontine migmatisation (e.g. Engi et al. 1995; Burri et
377 al. 2005). However, the 38-34 Ma UHP metamorphism in the Lepontine domain, is quickly
378 followed by a fast exhumation, then the UHT event and the final amphibolite faciès migmatisation
379 (Brouwer et al. 2004). This fast exhumation is related to a short-lived (less than 4 Ma) episode of
380 lithospheric thinning associated with a rise of hot asthenospheric material (Brouwer et al., 2004)
381 from 34 Ma to 32–30 Ma (Beltrando et al., 2010). Oalman et al. (2016) proposed that similar
382 lithospheric thinning associated with slab breakoff or roll back and asthenospheric upwelling could
383 also be responsible for the short-lived Alpine UHT metamorphism in the Gruf complex. A similar
384 geodynamic context is proposed for another example of Phanerozoic UHT metamorphism (16Ma)
385 of the island of Seram (Indonesia) where the UHT conditions were produced by slab rollback–
386 driven lithospheric extension and the exhumation of hot subcontinental lithospheric mantle
387 (Pownall et al, 2014; Pownall, 2015). Harley (2016) proposed that shorter duration UHT granulite
388 event can be formed as a consequence of severe lithospheric thinning and crustal extension
389 accompanied by voluminous magmatism in arc settings affected by subduction roll-back. Brouwer
390 et al. (2004) notice that heating by slab detachment is fast and transient (more than 100°C in up to
391 10 million years,), whereas radiogenic heating requires time spans of the order of tens of millions of
392 years and cessation of the subduction process. Finally, Perchuk et al. (2017) used numerical models
393 to explain ultra-hot orogeny and showed that UHT conditions at the bottom of the crust might be
394 produced by lateral propagation of the hot asthenospheric front during plate convergence associated
395 with lithospheric delamination. In this model, a close relationship of HT-UHT metamorphism with
396 tonalitic magmatism is proposed which could explain the relation between the Gruf UHT
397 metamorphism and the Bergell intrusion, which is one of the main Periadriatic igneous bodies
398 emplaced during Late Alpine times, characterised by an enriched mantle source (von Blanckenburg
399 et al., 1998), and interpreted as triggered by post-collisional slab break off.

400

401 **Conclusions**

402 In situ and in context zircon dating on zircon from a restitic granulite within charnockites give both
403 Permian-Triassic (304- 247 Ma) and Alpine ages (ca 34-30 Ma). $^{208}Pb/^{232}Th$ ages measured in
404 monazite from the same sample yield a weighted average age of 31.8 ± 0.3 Ma (MSWD = 3.2; N =
405 51) interpreted as the time of complete (re-)crystallisation of the monazite in equilibrium with the
406 UHT paragenesis. The Alpine UHT event was thus recorded by zircon rims and monazites. The

oldest ages we obtained in the zircons between 304 ± 12 Ma and 247 ± 6 Ma are interpreted as the age of the charnockitisation during which the precursor of the Al-Mg granulites of the Gruf complex acquired its restitic character. Our results show that the Gruf complex is the sole Penninic unit in the Central Alps recording the post Hercynian granulitic metamorphism which permits to reach and record UHT conditions during the Alpine cycle. The typical UHT paragenesis crystallised at Alpine time during a short-lived event (less than 5 Ma) related to lithospheric thinning associated with a rise of hot asthenospheric material.

Acknowledgments

References

Barker, F., 1964. Sapphirine-bearing rock, Val Codera, Italy. American Mineralogist 49, 146–152.

Barboza S.A. and Bergantz G.W. (2000) - Metamorphism and anatexis in the mafic complex contact aureole, Ivrea Zone, northern Italy. Journal of Petrology 41:1307–1327. https://doi.org/10.1093/petrology/41.8.1307

Beltrando M. , Lister G.S. , Rosenbaum G. , Richards S. and Forster M.A. (2010) - Recognizing episodic lithospheric thinning along a convergent plate margin: The example of the Early Oligocene Alps. Earth-Science Reviews 103; 81–98. https://doi.org/10.1016/j.earscirev.2010.09.001

Berger A., Rosenberg C., Schmid S.M. (1996) Ascent, emplacement and exhumation of the Bergell pluton within the Southern Steep Belt of the Central Alps. Schweizerische Mineralogische und Petrographische Mitteilungen 76:357–382.

Berger A., Rosenberg C., Schaltegger U. (2009) Stability and isotopic dating of monazite and allanite in partially molten rocks: examples from the Central Alps. Swiss Journal of Geoscience 102:15–29, https://doi.org/10.1007/s00015-009-1310-8

Bertotti G., Siletto G. B. & Spalla M. I. (1993) Deformation and metamorphism associated with crustal rifting: Permian to Liassic evolution of the Lake Lugano-Lake Como area (Southern Alps). Tectonophysics, 226, 271–284. Doi: 10.1016/0040-1951(93)90122-Z

Brodie K. H., Rex D. & Rutter E. H. (1989) On the age of deep crustal extensional faulting in the Ivrea zone, Northern Italy. Geological Society, London, Special Publications, 45, 203–210.

Doi: 10.1144/GSL.SP.1989.045.01.11

Brouwer F.M., van de Zedde D.M., Wortel M.J. and Vissers R.L. (2004) Late-orogenic heating during exhumation: Alpine PTt trajectories and thermomechanical models. Earth and Planetary Science Letters 220 (2004) 185-199. https://doi.org/10.1016/S0012-821X(04)00050-0

Brown M. 2007. Metamorphic conditions in orogenic belts: a record of secular change. International Geological Review, 49:193–234, https://doi.org/10.2747/0020-6814.49.3.193

Brown, M., (2008) - Granites, migmatites and residual granulites: relationships and processes. In: Sawyer, E.W., Brown, M. (Eds.), Working With Migmatites: Mineralogical Association of Canada Short Course, 38, pp. 97–144.

Burri T., Berger A., Engi M. (2005) Tertiary migmatites in the Central Alps: regional distribution, field relations, conditions of formation, and tectonic implications. Schweizerische Mineralogische und Petrographische Mitteilungen, 85:215–232

Clark C., Fitzsimons I.C.W., Healy D., Harley S.L. (2011) - How does the continental

crust get really hot? Elements 7: 235-240. https://doi.org/10.2113/gselements.7.4.235

Cornelius, H.P. (1916) Ein alpines Vorkommen von Sapphirine. Cent. Mineral., 265-269.

Cornelius, H.P. & Dittler E. (1929) Zur Kenntnis des Sapphirinvorkommens von Alpe Bresciadega in Val Codera (Italien, Prov. Sondrio). Neues Jahrbuch Fur Mineralogie-Abhandlungen, 59, 27-64.

Cherniak D.J., Watson B.E., Grove M., Harrison T.M. (2004) Pb diffusion in monazite: a combined RBS/SIMS study. Geochimica et Cosmochimica Acta 68:829–840. https://doi.org/10.1016/j.gca.2003.07.012

Didier A., Bosse V., Cherneva Z., Gautier P., Georgieva M., Paquette J.L. and Gerdjikov I. (2014). Syn-deformation fluid-assisted growth of monazite during renewed high-grade metamorphism in metapelites of the Central Rhodope (Bulgaria, Greece) Chemical Geology 381, 206–222. https://doi.org/10.1016/j.chemgeo.2014.05.020

Davies J.H. & Von Blanckenburg F. (1995) Slab breakoff: A model of lithosphere detachment and its test in the magmatism and deformation of collisional orogens. Earth and Planetary Science Letters, 129, 85–102. Doi: 10.1016/0012-821X(94)00237-S

Didier A., Bosse V., Bouloton J., Mostefaoui S., Viala M., Paquette J.L., Devidal J.L., Duhamel R. (2015). NanoSIMS mapping and LA‐ICP‐MS chemical and U–Th–Pb data in monazite from a xenolith enclosed in ndesite (Central Slovakia Volcanic Field). Contribution to Mineralogy & Petrology vol.170, p.45, doi:10.1007/s00410-015-1200-1.

Diella V., Spalla M. I. & Tunesi, A. (1992) Contrasted thermo-mechanical evolutions in the Southalpine metamorphic basement of the Orobic Alps (Central Alps, Italy). Journal of Metamorphic Geology, 10, 203–219. Doi: 10.1111/j.1525-1314.1992.tb00079.x

Droop G.T.R. & Bucher-Nurminen K. (1984) Reaction textures and metamorphic evolution of sapphirine-bearing granulites from the Gruf Complex, Italian Central Alps. Journal of Petrology, 25, 766-803.

Engi, M., Todd, C.S., Schmatz, D.R., 1995. Tertiary metamorphic conditions in the eastern Lepontine Alps. Schweizerische Mineralogische und Petrographische Mitteilungen 75, 347– 369.

Engi M., Bousquet R. & Berger A. (2004) Explanatory notes to the map: Metamorphic structure of the Alps - Central Alps. Mitteilungen der Österreichischen Mineralogischen Gesellschaft, 149, 157-173.

Galli A., Le Bayon B., Schmidt M.W., Burg J.P., Caddick M.J., Reusser E. (2011) Granulites and charnockites of the Gruf Complex: evidence for Permian ultra-high temperature metamorphism in the Central Alps. Lithos 124:17–45. doi:10.1016/j.lithos.2010.08.003

Galli, A., Le Bayon, B., Schmidt, M.W., Burg, J.P., Reusser, E., Sergeev, S.A., & Larionov, A. (2012). U-Pb zircon dating of the Gruf Complex: disclosing the late Variscan granulitic lower crust of Europe stranded in the Central Alps. Contributions to Mineralogy and Petrology, 163(2), 353–378. DOI 10.1007/s00410-011-0676-6

Galli A., Le Bayon B., Schmidt M.W., Burg J.P. & Reusser E. (2013) Tectonometamorphic history of the Gruf complex (Central Alps): exhumation of a granulite–migmatite complex with the Bergell pluton. Swiss Journal of Geoscience, 106:33–62. DOI 10.1007/s00015-013-0120-1

Guevara V.E. & Caddick M.J. (2016) Shooting at a moving target: phase equilibria modelling of high temperature metamorphism. Journal of metamorphic Geology, 34, 209–235. doi:10.1111/jmg.12179

Harley S.L. (1998). – On the occurrence and characterization of ultrahightemperature crustal metamorphism. *In*: Treloar, P.J., O'Brien, P.J. (Eds.), What Drives Metamorphism and Metamorphic Relations? *Geological Society, London, Special Publication*, **138**, p. 81-107.

Harley S.L. (2016) – A matter of time: the importance of the duration of UHT metamorphism.

494 Journal of Mineralogical and Petrological Sciences, v. 111, p. 50-72. doi:10.2465/jmps.160128

495 Kelly N. M., Harley S. L., & Möller A. (2012). Complexity in the behavior and recrystallization of
496 monazite during high-T metamorphism and fluid infiltration. Chemical Geology, 322–323, 192–
497 208. https://doi.org/10.1016/j.chemgeo.2012.07.00

498 Kelsey D.E., and Hand M. (2015) - On ultrahigh temperature crustal metamorphism: Phase equilibr
499 ia, trace element thermometry, bulk composition, heat sources, timescales and tectonic settings.
500 Geoscience Frontiers 6, 311 – 356. http://dx.doi.org/10.1016/j.gsf.2014.09.006

501 Kelsey D.E., White R.W., Powell R. (2003) – Orthopyroxene-sillimanite-quartz
502 assemblages: distribution, petrology, quantitative P-T-X constraints and P-T paths. Journal of
503 Metamorphic Geology 21, 439-453. DOI: 10.1046/j.1525-1314.2003.00456.x

504 Köppel V., Günthert A., Grünenfelder M. (1981). Patterns of U–Pb zircon and monazite ages in
505 polymetamorphic units of the Swiss Alps. Schweizerische Mineralogische und Petrographische
506 Mitteilungen 61, 97–119.

507 Korhonena F.J., Clarka C., Brown M., Bhattacharyac S., Taylora R. (2013) How long-lived is
508 ultrahigh temperature (UHT) metamorphism? Constraints from zircon and monazite geochronology
509 in the Eastern Ghats orogenic belt, India. Precambrian Research. Vol. 234, 322-350.
510 doi.org/10.1016/j.precamres.2012.12.001

511 Lardeaux J.M. and Spalla I. (1991) - From granulites to eclogites in the Sesia zone (Italian Western
512 Alps): a record of opening and closure of the Piedmont ocean. Journal of Metamorphic Geology,
513 9:35–59

514 Liati A., Gebauer D. (2003) Geochronological constraints for the time of metamorphism in the Gruf
515 Complex (Central Alps) and implications for the Adula-Cima Lunga nappe system. Schweizerische
516 Mineralogische und Petrographische Mitteilungen, 83:159–172

517 McDade P., Harley S.L. (2001) - A petrogenetic grid for aluminous granulite facies metapelites in
518 the KFMASH system. Journal of Metamorphic Geology, p. 19, p. 45 – 59 DOI: 10.1046/j.0263-
519 4929.2000.00296.x

520 Manzotti P., Rubatto D., Darling J., Zucali M., Cenki-Tok B., Engi M. (2012) - From Permo-
521 Triassic lithospheric thinning to Jurassic rifting at the Adriatic margin: Petrological and
522 geochronological record in Valtournenche (Western Italian Alps). Lithos 146–147; 276–292.
523 doi:10.1016/j.lithos.2012.05.007

524 Manzotti, P. & Zucali, M. 2013. The pre-Alpine tectonic history of the Austroalpine continental
525 basement in the Valpelline unit (Western Italian Alps). Geological Magazine, 150, 153–172. Doi:
526 10.1017/S0016756812000441.

527 Marotta A.M., Roda M., Conte K., Spalla M.I. (2016) Thermo-mechanical numerical model of the
528 transition from continental rifting to oceanic spreading: the case study of the Alpine Tethys.
529 Geological Magazine, in press, 1-30. Doi: 10.1017/S0016756816000856.

530 Marotta A.M., Gosso G., Spalla M.I. (2009) Upper and lower crustal evolution during lithospheric
531 extension: Numerical modelling and natural footprints from the European Alps. Geological Society
532 Special Publication, 321, 33-72. Doi: 10.1144/SP321.3.

533 Montel J.M.(1986) Experimental determination of the solubility of Ce-monazite in Si02-Al203-
534 K20-Na20 melts at 800 °C, 2 kbar,under h2O-saturated conditions Geology v. 14 no. 8 p. 659-662

535 Montel J.M., Didier J. & Pichavant M. (1991) Origin of surmicaceous enclaves in intrusive
536 granites. Developments in Petrology : Enclaves and Granite Petrology, 509-528. Elsevier.

537 Müntener O., Hermann J. & Trommsdorff V. (2000). Cooling history and exhumation of lower
538 crustal granulite and upper Mantle (Malenco, eastern Central Alps). Journal of Petrology, 41, 175–
539 200.

Niggli E. (1974) Metamorphism and tectonics of the Alps. Memorie della Società geologica Italiana, 13, 285-289.

Oalmann J., Möller A. & Bousquet R., (2013). P-T modelling reveals juxtaposition of units within the Gruf Complex (Central Alps) during orogenesis. Mineralogical Magazine, 77, 1873. DOI:10.1180/minmag.2013.077.5.15

Oalmann J. Möller A. & Bousquet R., (2016) – Unravelling the P-T-t evolution of the crust of the Gruf complex by in situ accessory mineral dating and thermometry combined with P-T modelling of microdomains. European Mineralogical Conference, Rimini.

Paquette J.L., Goncalves P., Devouard B. and Nicollet C. (2004). Micro-drilling ID-TIMS U-Pb dating of single monazites: A new method to unravel complex poly-metamorphic evolutions. Application to the UHT granulites of Andriamena (North-Central Madagascar). Contributions to Mineralogy and Petrology, 147: 110–122 DOI: 10.1007/s00410-003-0549-8

Paquette, J.-L., Tiepolo, M., 2007. High resolution (5 µm) U-Th-Pb isotopes dating of monazite with excimer laser ablation (ELA)-ICPMS. Chemical Geology 240, 222–237. DOI:10.1016/j.chemgeo.2007.02.014

Paquette, J.L., Piro, J.L., Devidal, J.L., Bosse, V., Didier, A., 2014. Sensitivity enhancement in LA-ICP-MS by N2 addition to carrier gas: application to radiometric dating of U-Th bearing minerals. Agilent ICP-MS J. 58, 4–5

Perchuk A.L., Safonov O.G.,. Smit C.A,. van Reenen D.D,. Zakharov V.S, Gerya T.V. (2017) Precambrian ultra-hot orogenic factory: Making and reworking of continental crust; Tectonophysics, in press. https://doi.org/10.1016/j.tecto.2016.11.041

Peressini G., Quick J. E., Sinigoi S., Hofmann A. W. & Fanning M. (2007) Duration of a large mafic intrusion and heat transfer in the lower crust: a SHRIMPU–Pb zircon study in the Ivrea-Verbano Zone (Western Alps, Italy). Journal of Petrology, 48, 1185–1218. Doi: 10.1093/petrology/egm014

Pownall J.M. (2015) - UHT metamorphism on Seram, eastern Indonesia: reaction microstructures and P–T evolution of spinel-bearing garnet–sillimanite granulites from the Kobipoto Complex. Journal of metamorphic Geology, 33, 909–935 doi:10.1111/jmg.12153

Pownall J.M., Hall R., Armstrong R.A. & Forster M.A. (2014) - Earth's youngest known ultrahigh-temperature granulites discovered on Seram, eastern Indonesia. Geology, 42, 279–282. DOI: https://doi.org/10.1130/G35230.1

Rapp R.P. & Watson E.B. (1986). Monazite solubility and dissolution kinetics: implications for the thorium and light rare earth chemistry of felsic magmas. Contributions to Mineralogy and Petrology. 94 : 304-316.

Redler C., White R.W., Johnson. T.E., (2013) Migmatites in the Ivrea Zone (NW Italy): Constraints on partial melting and melt loss in metasedimentary rocks from Val Strona di Omegna Lithos Vol. 190–191, March 2014, Pages 1-12. doi.org/10.1016/j.lithos.2013.04.019

Rocha B.C., Moraes R., Möller A., Cioffi C.R., Jercinovic M.J. (2017) Timing of anatexis and melt crystallization in the Socorro–Guaxupé Nappe, SE Brazil: Insights from trace element composition of zircon, monazite and garnet coupled to UPb geochronology. Lithos 277, 337-355. https://doi.org/10.1016/j.lithos.2016.05.020

Rubatto D., Hermann J., Buick I.S., (2006). Temperature and bulk composition control on the growth of monazite and zircon during low-pressure anatexis (Mount Stafford, central Australia). Journal of Petrology, 47, 1973–1996. https://doi.org/10.1093/petrology/egl033

Rubatto D., Chakraborty S. and Dasgupta S. (2013) Timescales of crustal melting in the Higher Himalayan Crystallines (Sikkim, Eastern Himalaya) inferred from trace element-constrained monazite and zircon chronology. Contributions to Mineralogy and Petrology 165:349–372. doi: 10.1007/s00410-012-0812-y

Rubatto D., Hermann J., Berger A., Engi M., 2009. Protracted fluid-present melting during Barrovian metamorphism in the Central Alps. Contributions to Mineralogy and Petrology. doi:10.1007/s00410-009-0406-5.

Schaltegger U. (1994) Unravelling the pre-Mesozoic history of Aar and Gotthard massifs (Central Alps) by isotopic dating - a review. Schweizerische Mineralogische und Petrographische Mitteilungen, 74, 41–51.

Schärer U. (1984) The effect of initial 230Th disequilibrium on young U-Pb ages: the Makalu case, Himalaya. Earth Planetary Science Letters 67 : 191-0204.

Schmid S.M., Berger A., Davidson C., Gieré R., Hermann J., Nievergelt P., Pusching A.R. & Rosenberg C. (1996) The Bergell Pluton (Southern Switzerland-Northern Italy): overview accompanying a geological-tectonic map of the intrusion and surrounding country rocks. Schweizerische Mineralogische und Petrographische Mitteilungen, 76, 329–355.

Schmitz S., Möller A., Wilke M., Malzer W., Kannigiesser B., Bousquet R., Berger A., Schefer S. (2009) Chemical U-Th-Pb dating of monazite by 3D-Micro X-ray fluorescence analysis with synchrotron radiation. European Journal of Mineralogy 21:927–945. https://doi.org/10.1127/0935-1221/2009/0021-1964

Schuster R., Scharbert S., Abart R. & Frank W. (2001) Permo-Triassic extension and related HT/LP metamorphism in the Austroalpine-Southalpine realm. Mitteilungen der Gesellschaft der Geologie und Bergbaustudenten in Österreich, 45, 111–141.

Schuster R. & Stuewe K. (2008) Permian metamorphic event in the Alps. Geology, 36, 603–606. Doi: 10.1130/G24703A.1.

Spalla M. I. & Marotta A. M. (2007) P–T evolutions vs. numerical modelling: a key to unravel the Paleozoic to early-Mesozoic tectonic evolution of the Alpine area. Periodico di Mineralogia, 76, 267–308. Doi: 10.2451/2007PM0029.

Spalla M. I., Zanoni D., Marotta A. M., Rebay G., Roda M., Zucali M. & Gosso G. (2014) The transition from Variscan collision to continental break-up in the Alps: insights from the comparison between natural data and numerical model predictions. Geological Society, London, Special Publication, 405, 363–400. Doi: 10.1144/SP405.11

Spear F.S., Pyle J.M. (2002) Apatite, monazite, and xenotine in metamorphic rocks, reviews in mineralogy and geochemistry, phosphates: geochemical, geobiological, and materials importance. Mineralogical Society of America, 48:523–558.

Stepanov A.S., Hermann J., Rapp R.P., Rubatto D. (2012) Experimental study of monazite/melt partitioning with implications for the REE, Th and U geochemistry of crustal rocks. Chemical Geology. 300-301:200–220. https://doi.org/10.1016/j.chemgeo.2012.01.007

Stüwe K. 1995 - Thermal buffering effects at the solidus. Implications for the equilibration of partially melted metamorphic rocks. Tectonophysics vol. 248 p. 39-51.

Todd, C.S. and Engi, M., 1997. Metamorphic field gradients in the Central Alps. Journal of Metamorphic Geology 15, 513–530

Tribuzio R., Thirlwall M.F., Messiga B. (1999) Petrology, mineral and isotope geochemistry of the Sondalo gabbroic complex (Central Alps, Northern Italy): implications for the origin of post-Variscan magmatism. Contributions to Mineralogy and Petrology, 136: 48 – 62.

Trommsdorff V., (1966). Progressive Metamorphose kieseliger Karbonatgesteine in den Zentralalpen zwischen Bernina und Simplon. Schweizerische Mineralogische und Petrographische Mitteilungen 46, 431–460.

Vavra G. and Schaltegger, U. (1999) - Post-granulite facies monazite growth and rejuvenation during Permian to Lower Jurassic thermal and fluid events in the Ivrea Zone (Southern Alps. Contributions to Mineralogy and Petrology, 134: 405 – 414

Vielzeuf, D. and Holloway, J.R. (1988). Experimental determination of the fluid-absent melting reactions of pelitic rocks — consequences for the crustal differentiation. Contributions to Mineralogy and Petrology, 98, 257–276.

Von Blanckenburg F. & Davies J.H. (1995) Slab breakoff. A model for syncollisional magmatism and tectonics in the Alps. Tectonics, 14, 120–131. Doi: 10.1029/94TC02051

Wenk H.R., Wenk E. and Wallace J.H. (1974) Metamorphic mineral assemblages in politic rocks of the Bergell Alps. Schweizerische Mineralogische und Petrographische Mitteilungen, 54:507-554

Whitney D.L. & Evans B.W., 2010. Abbreviations for names of rock-forming minerals. American Mineralogist, 95, 185–187. DOI: 10.2138/am.2010.3371

Figures captions

Fig.1: Sketch map of the Gruf complex in the eastern Central Alps after Galli et al., (2011); Asterisk locates upper Val Codera. The sketch is located in the Alpine chain (inset).

Fig. 2: Microphotographs of the parageneses and textures of the granulitic rock (Plane-(PPL) and cross (XPL)-polarized light; (**a**): The Spr bearing granulitic paragenesis (PPL); (**b**): Complex retrograde symplectites in the Spr bearing portion of the rock granulite with spr2, sp, cord, sil2. Opx + Crd symplectites replace Grt (PPL); (**c**): Spr2+crd resulting of the retrograde reaction Opx + Sil = Spr + Crd (PPL); (**d**): the charnockitic paragenesis (XPL); (**e**): textures of incipient melting or residual melt after extraction in the charnockite portion of the rock (XPL). Abbreviations in text and figures are from Whitney and Evans (2010).

Fig. 3: Al_2O_3 profiles in the primary Opx (C: core and R: rim) and Al2O3 concentrations (contents values) in the Opx from the Opx + Crd symplectite (sym) around garnet.

Fig. 4 (**a**): Resorbed crystals of zircons included in primary phenocrysts, Spr and Sil (PPL); (**b**): Cathodoluminescence images of zircons in the Crd – Bt matrix with oscillatory zoning; (**c**): zircon grains surrounded by highly luminescent rim (<5 µm to 15 µm) with euhedral faces with Alpine or intermediate ages ($^{206}Pb/^{238}U$ ages; 2σ)

Fig. 5 (**a**): Monazite inclusions in the phenocrysts (PPL) of Sapphirine and Al-rich orthopyroxene of the Spr bearing domain of the rock; (**b**): Monazite inclusions in an Opx of the charnockite portion of the rock; note the tiny overgrowths (rich in Y) in the BSE image (crystal T14M1). Circles: $^{208}Pb/^{232}Th$ ages in Ma (with ±1.1 Ma for all data).

Fig. 6 (**a**): BSE images of figure 2b and of the monazites in Spr, Crd and in clusters in late symplectites; cathodoluminescence of a zircon in Crd. ThO_2 and Y_2O_3 X-ray maps (spots; in wt%) in the crystal T50M1 and $^{208}Pb/^{232}Th$ ages (circles) ages in Ma (with ±1.1 Ma for the monazites). Black inclusions are needles of sillimanite; arrows: diamond-shaped basal sections.

Fig. 6 (**b**): ThO_2 and Y_2O_3 X-ray maps (spots; in wt%) and BSE image and $^{208}Pb/^{232}Th$ ages (circles) ages in Ma with ±1.1Ma for a monazite in the charnockite portion of the rock (crystal T12M1).

Fig. 7: Chemical composition of the monazites; (**a**): Ternary diagram showing the relative Y_2O_3, ThO_2 and UO_2 (wt%) contents; (**b**): Y_2O_3 versus Gd_2O_3; (**c**): La_2O_3 versus Gd_2O_3.

Fig. 8: Geochronological results; (**a**): $^{208}Pb/^{232}Th$ versus $^{206}Pb/^{238}U$ diagram for the monazite; (**b**): Weighted average $^{208}Pb/^{232}Th$ ages in monazite; (**c**): Tera Wasserburg diagram showing the zircon and monazite data (for more clarity, only concordant U/Pb data are shown); (**d**): Tera Wasserburg diagram showing U/Pb results for zircon cores with U content ≤ 1000 ppm and zircon grain without apparent Alpine rim in CLI.

Table 1: Electron microprobe analyses of the monazites. G = granulite domain; Ch = charnockite domain.

Table

Click here to download Table Table1-Mnz.xls

Table 1 : analyses of monazites.

	G	G		G	G			Ch			G		Ch		G		G	G	G	G
Analyses	**2**	**7**	**14**	**17**	**18**	**23**	**25**	**32**	**33**	**34**	**42**	**45**	**49**	**53**	**56**	**57**	**58**	**59**	**61**	**64**
	T50 - M2	T50-M1		i saphirine	T50 - cluster			T14 M1			T13 M1		T12-M1		T10bis-M2		T10 bis	T10bisM1	T18-i OPX	T33-i OPX
SiO2	0.17	0.27	0.12	0.19	0.21	0.10	0.16	0.25	0.31	0.47	0.22	0.38	0.39	0.59	0.41	0.32	0.19	1.34	0.19	0.32
P2O5	30.15	29.51	29.77	29.54	29.93	29.99	29.67	30.20	29.96	29.65	30.29	29.57	30.02	29.09	29.60	29.57	29.80	27.70	29.65	30.12
Ce2O3	29.92	28.92	30.59	29.74	29.23	30.28	29.79	25.18	25.44	25.61	28.36	25.20	24.73	25.71	29.57	29.48	29.22	30.89	29.94	27.14
La2O3	13.58	13.48	14.31	13.26	13.14	13.30	13.59	10.70	11.09	11.10	12.51	11.39	10.70	11.22	13.47	13.39	13.20	14.78	13.59	12.29
Pr2O3	3.30	3.18	3.10	3.39	3.19	3.45	3.21	2.78	2.98	2.87	2.93	3.01	2.77	2.89	3.08	3.09	3.23	3.65	3.05	3.02
Nd2O3	11.49	10.97	11.95	11.58	11.36	11.32	11.06	9.88	10.44	10.49	10.75	8.71	10.32	11.27	11.65	11.66	10.92	11.99	10.52	11.02
Sm2O3	1.95	1.46	1.54	1.66	1.74	2.17	1.66	2.14	1.90	2.03	1.92	1.64	1.85	1.82	1.73	1.52	1.75	1.19	1.77	1.74
Gd2O3	1.33	0.44	0.69	1.09	1.54	1.58	1.06	2.44	1.91	2.05	1.39	1.01	2.04	1.60	1.07	1.11	1.01	0.64	0.91	1.82
Y2O3	0.39	0.13	0.35	0.31	0.50	0.69	0.32	4.78	3.78	3.24	0.98	0.47	3.89	2.63	0.27	0.58	0.91	0.14	0.65	2.14
CaO	1.34	1.75	1.16	1.39	1.45	1.15	1.46	1.61	1.76	1.77	1.83	2.90	1.78	1.67	1.31	1.45	1.53	0.44	1.53	1.49
ThO2	5.79	8.43	5.15	6.42	6.07	3.92	6.73	7.84	8.75	9.32	6.78	10.82	9.59	10.07	7.17	5.74	5.19	6.96	5.48	8.00
UO2	0.98	0.33	0.50	0.78	0.83	1.35	0.75	0.74	0.41	0.32	2.05	3.50	0.40	0.26	0.45	1.29	2.01	0.20	1.78	0.37
PbO	0.03	0.00	0.00	0.04	0.01	0.00	0.00	0.00	0.03	0.00	0.01	0.02	0.00	0.01	0.00	0.00	0.01	0.00	0.03	0.01
Total	**100.41**	**98.87**	**99.23**	**99.38**	**99.20**	**99.30**	**99.48**	**98.54**	**98.76**	**98.93**	**100.00**	**98.63**	**98.49**	**98.83**	**99.76**	**99.21**	**98.96**	**99.90**	**99.08**	**99.47**
Si	0.007	0.011	0.005	0.007	0.008	0.004	0.007	0.010	0.012	0.018	0.009	0.015	0.015	0.023	0.016	0.013	0.007	0.054	0.008	0.012
P	0.996	0.991	0.995	0.990	0.997	0.999	0.992	0.995	0.991	0.984	0.998	0.990	0.993	0.975	0.987	0.988	0.995	0.941	0.992	0.995
Ce	0.427	0.420	0.442	0.431	0.421	0.436	0.431	0.359	0.364	0.368	0.404	0.365	0.354	0.373	0.426	0.426	0.422	0.454	0.433	0.388
La	0.195	0.197	0.208	0.194	0.191	0.193	0.198	0.154	0.160	0.161	0.179	0.166	0.154	0.164	0.196	0.195	0.192	0.219	0.198	0.177
Pr	0.047	0.046	0.045	0.049	0.046	0.049	0.046	0.039	0.042	0.041	0.042	0.043	0.039	0.042	0.044	0.044	0.046	0.053	0.044	0.043
Nd	0.160	0.155	0.169	0.164	0.160	0.159	0.156	0.137	0.146	0.147	0.149	0.123	0.144	0.159	0.164	0.164	0.154	0.172	0.149	0.153
Sm	0.026	0.020	0.021	0.023	0.024	0.029	0.023	0.029	0.026	0.027	0.026	0.022	0.025	0.025	0.023	0.021	0.024	0.016	0.024	0.023
Eu	0.000	0.000	0.000	0.000	0.000	0.000	0.000	0.000	0.000	0.000	0.000	0.000	0.000	0.000	0.000	0.000	0.000	0.000	0.000	0.000
Gd	0.017	0.006	0.009	0.014	0.020	0.021	0.014	0.031	0.025	0.027	0.018	0.013	0.026	0.021	0.014	0.015	0.013	0.009	0.012	0.023
Y	0.008	0.003	0.007	0.006	0.010	0.015	0.007	0.099	0.079	0.068	0.020	0.010	0.081	0.055	0.006	0.012	0.019	0.003	0.014	0.044
Ca	0.056	0.074	0.049	0.059	0.061	0.048	0.062	0.067	0.074	0.075	0.076	0.123	0.074	0.071	0.055	0.062	0.064	0.019	0.065	0.062
Th	0.051	0.076	0.046	0.058	0.054	0.035	0.060	0.069	0.078	0.083	0.060	0.097	0.085	0.091	0.064	0.052	0.047	0.064	0.049	0.071
U	0.008	0.003	0.004	0.007	0.007	0.012	0.007	0.006	0.004	0.003	0.018	0.031	0.004	0.002	0.004	0.011	0.018	0.002	0.016	0.003
Pb	0.000	0.000	0.000	0.000	0.000	0.000	0.000	0.000	0.000	0.000	0.000	0.000	0.000	0.000	0.000	0.000	0.000	0.000	0.000	0.000
Summe	**2.000**	**2.001**	**2.001**	**2.002**	**1.999**	**2.000**	**2.001**	**1.997**	**1.999**	**2.001**	**1.998**	**2.000**	**1.995**	**2.001**	**1.999**	**2.003**	**2.001**	**2.006**	**2.003**	**1.995**

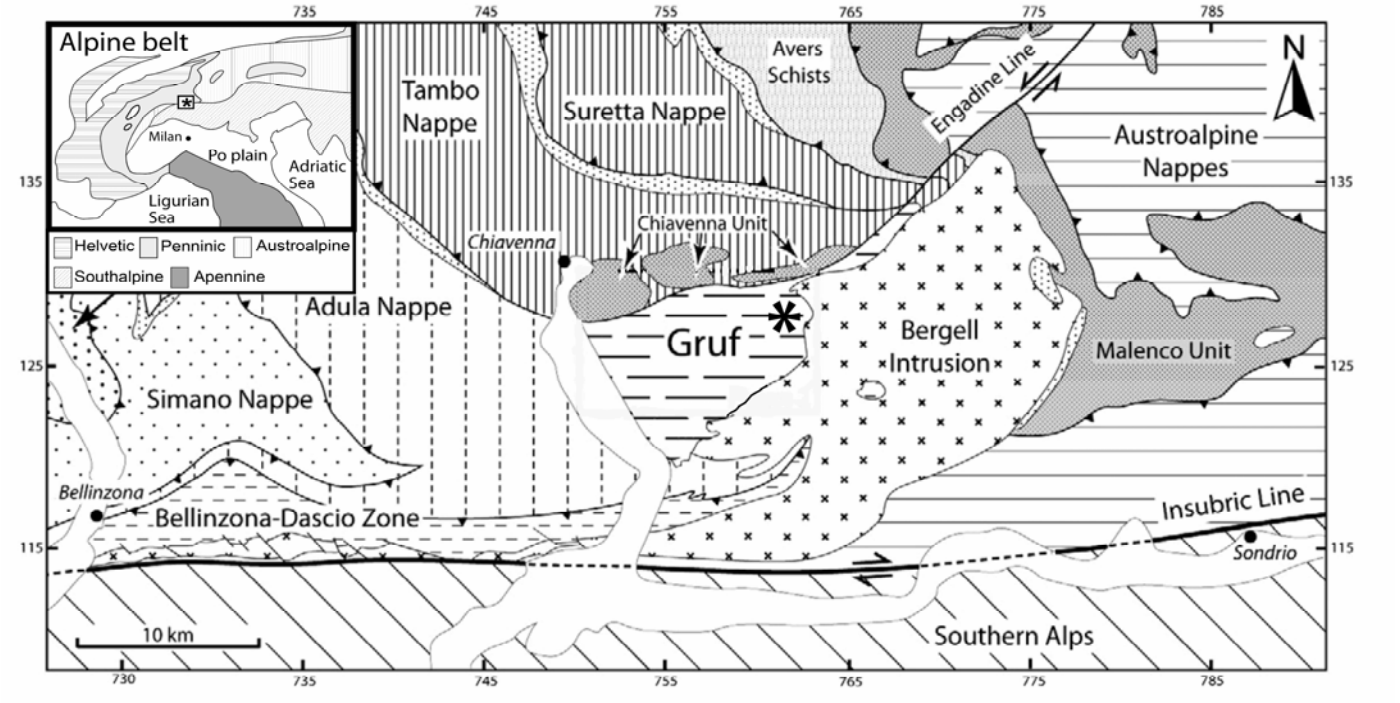

Figure 1

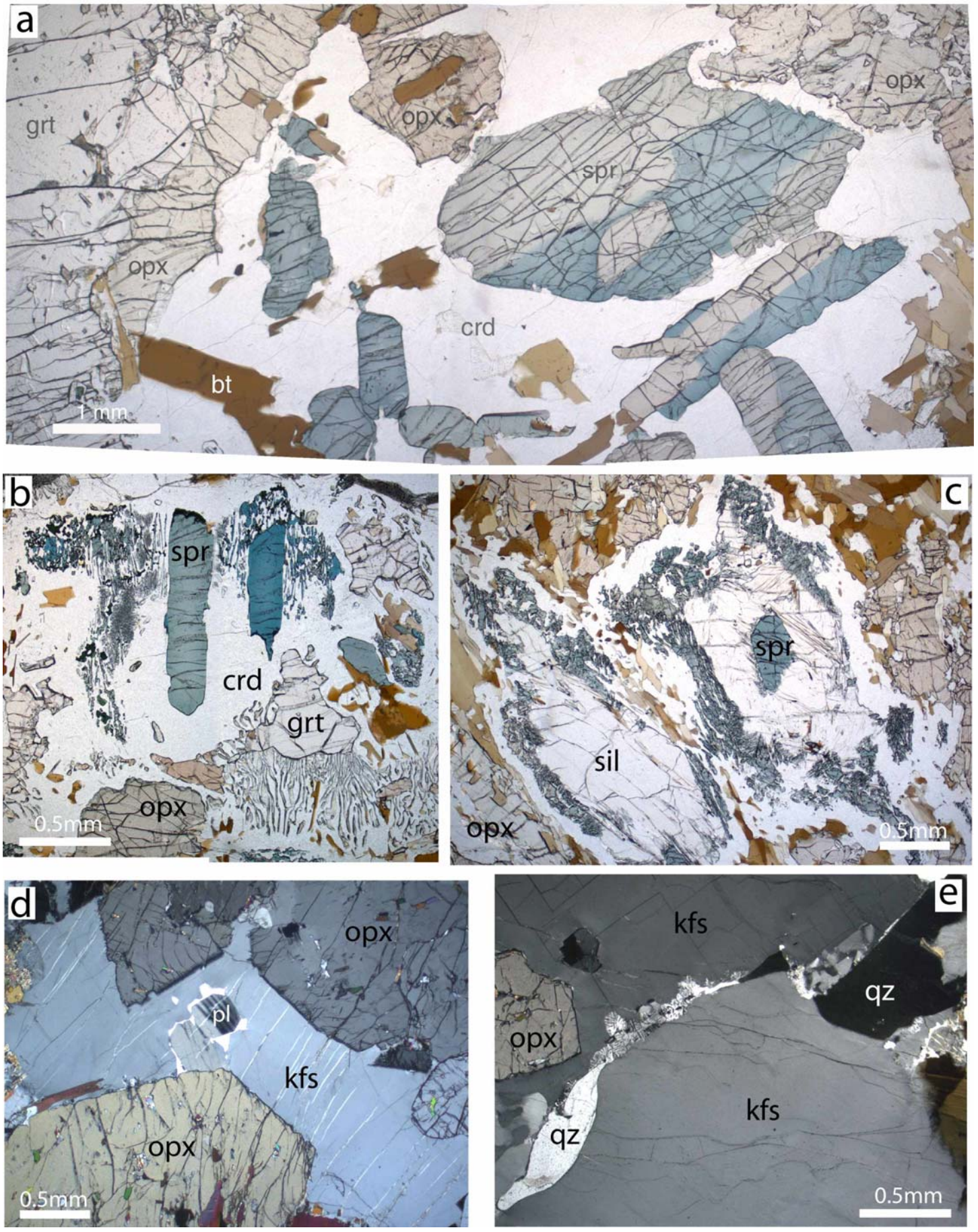
a
grt
opx
opx
spr
opx
crd
bt
1 mm
b
spr
crd
grt
opx
0.5mm
c
spr
sil
opx
0.5mm
d
opx
pl
kfs
opx
0.5mm
e
kfs
qz
opx
kfs
qz
0.5mm

Figure 2

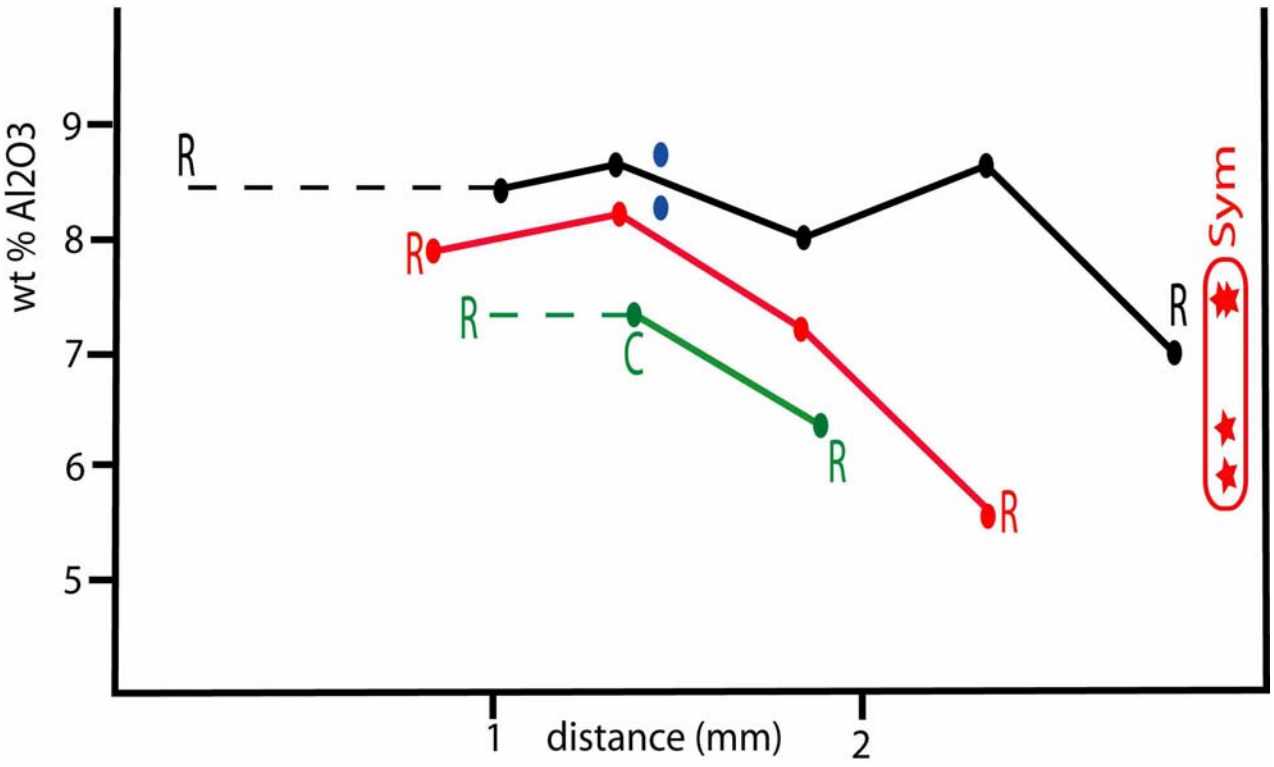

Figure 3

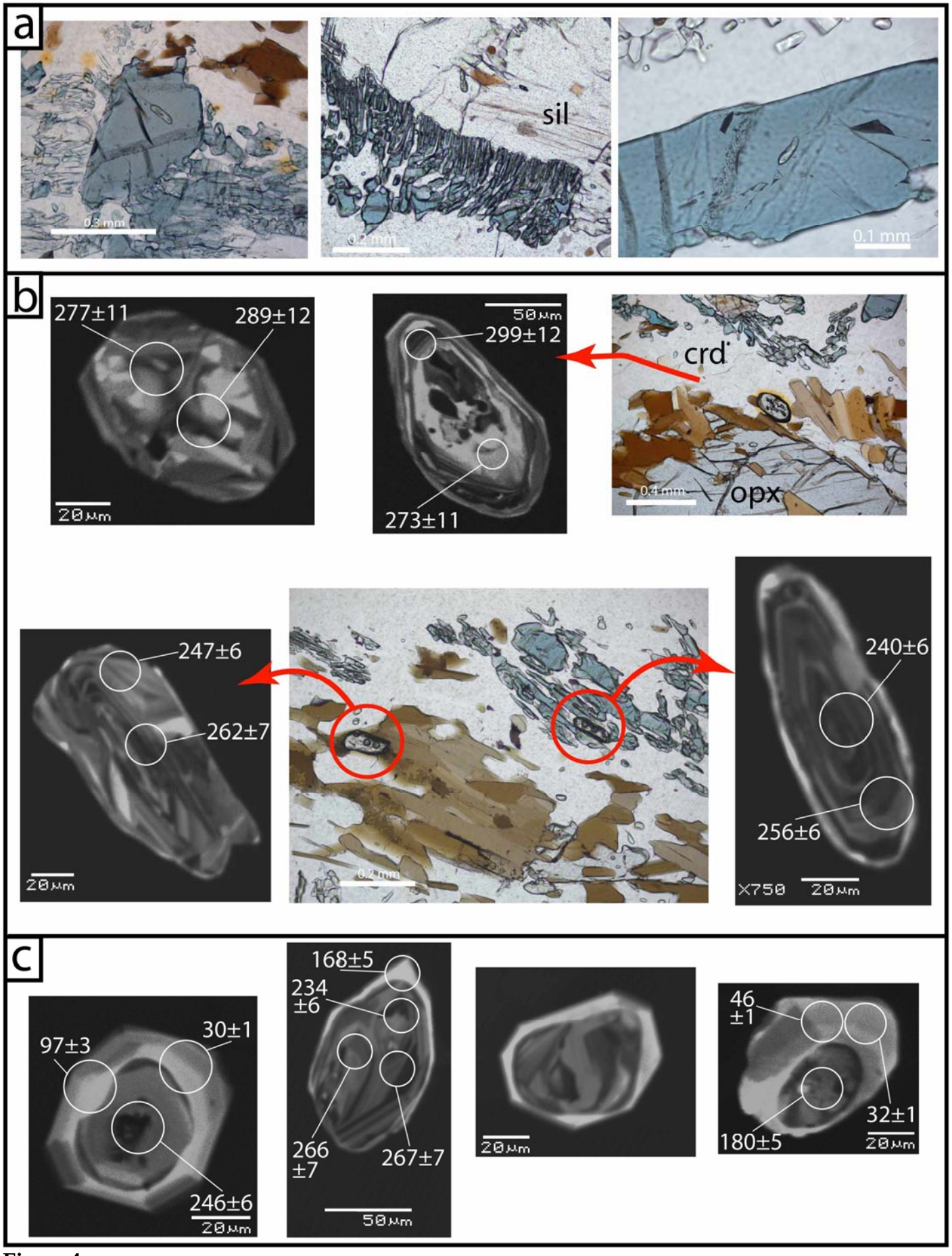
a
0.3 mm
sil
0.2 mm
0.1 mm
b
277±11
289±12
20 µm
50 µm
299±12
273±11
crd
0.4 mm
opx
247±6
262±7
20 µm
0.2 mm
240±6
256±6
X750
20 µm
c
97±3
30±1
246±6
20 µm
168±5
234
±6
266
±7
267±7
50 µm
20 µm
46
±1
32±1
180±5
20 µm

Figure 4

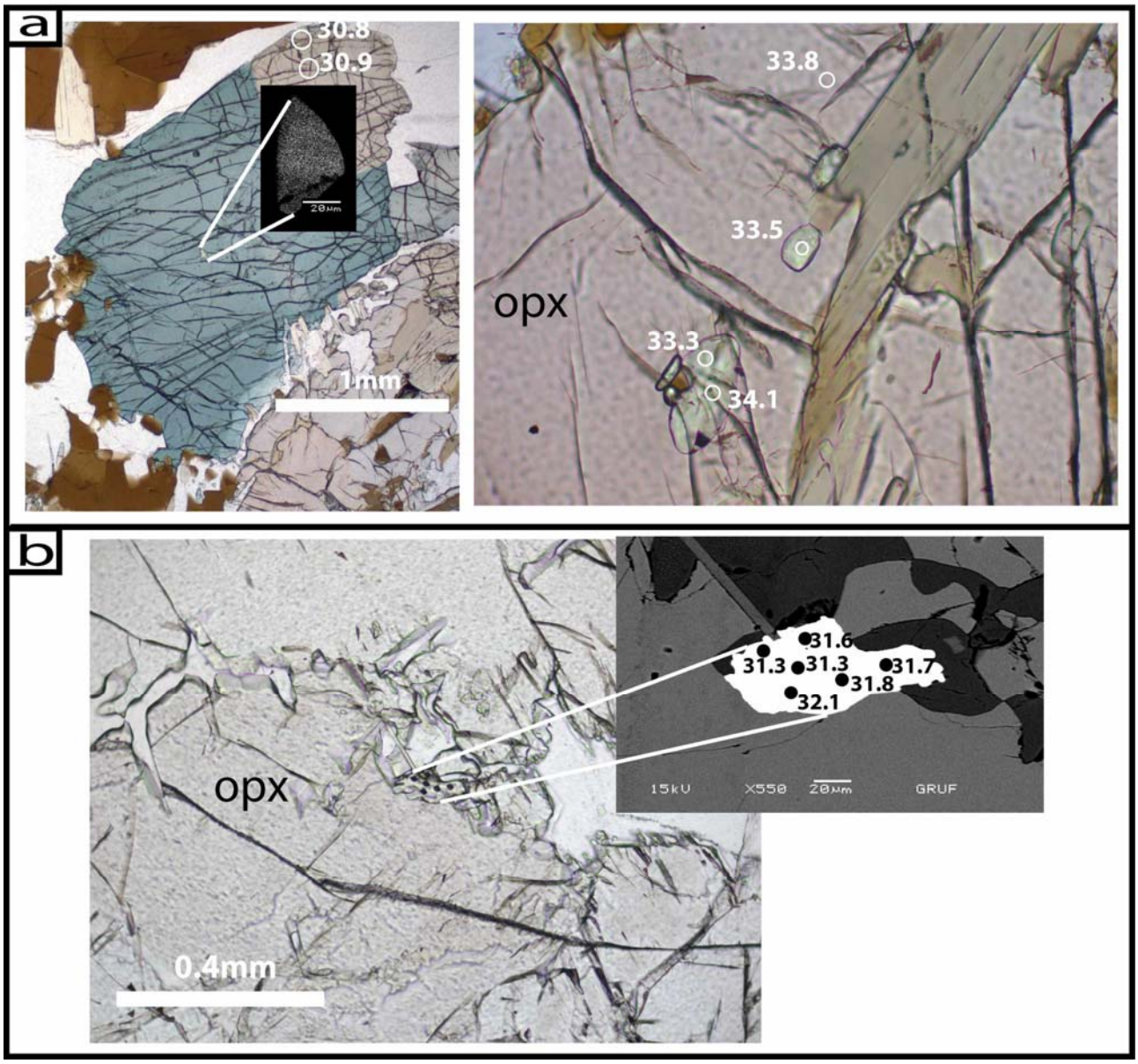
a
30.8
30.9
20µm
1mm
33.8
33.5
opx
33.3
34.1
b
opx
0.4mm
31.6
31.3
31.3
31.7
31.8
32.1
15kV
X550
20µm
GRUF

Figure 5

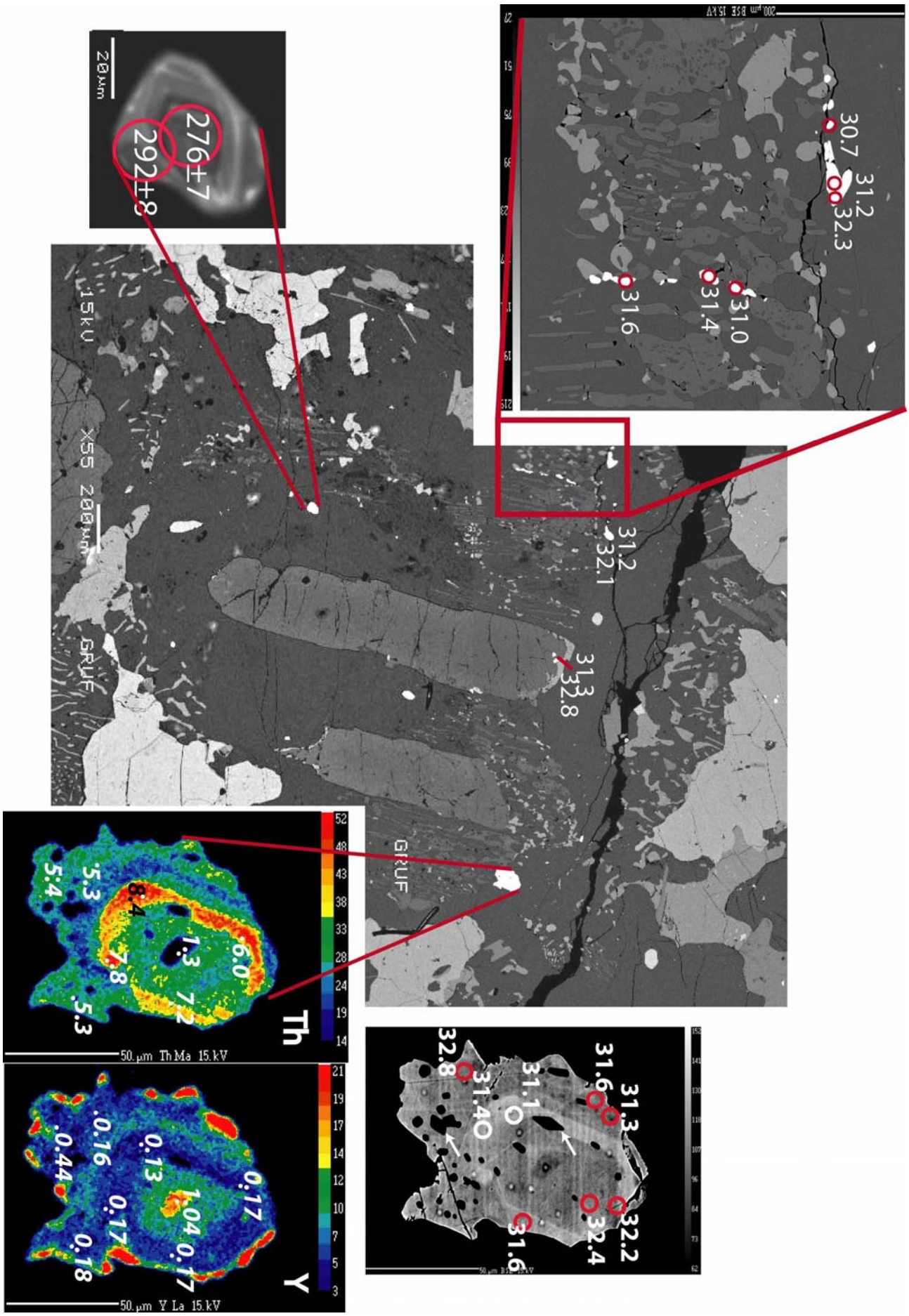
20 µm
276±7
292±8
15kV
X55 200µm
GRUF
30.7
31.2
32.3
31.6
31.4
31.0
31.2
32.1
31.3
32.8
GRUF
Th
50. µm Th Ma 15.kV
Y
50. µm Y La 15.kV

Figure 6a

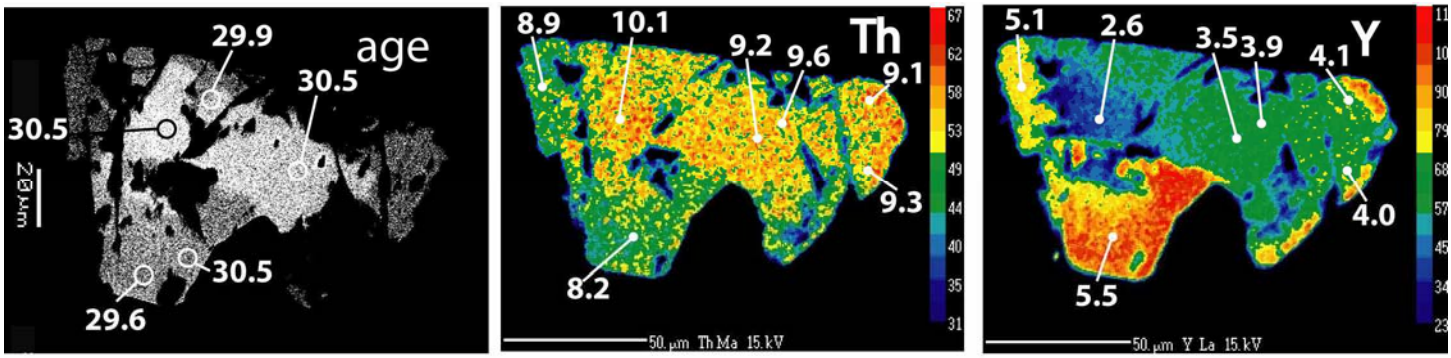

Figure 6b

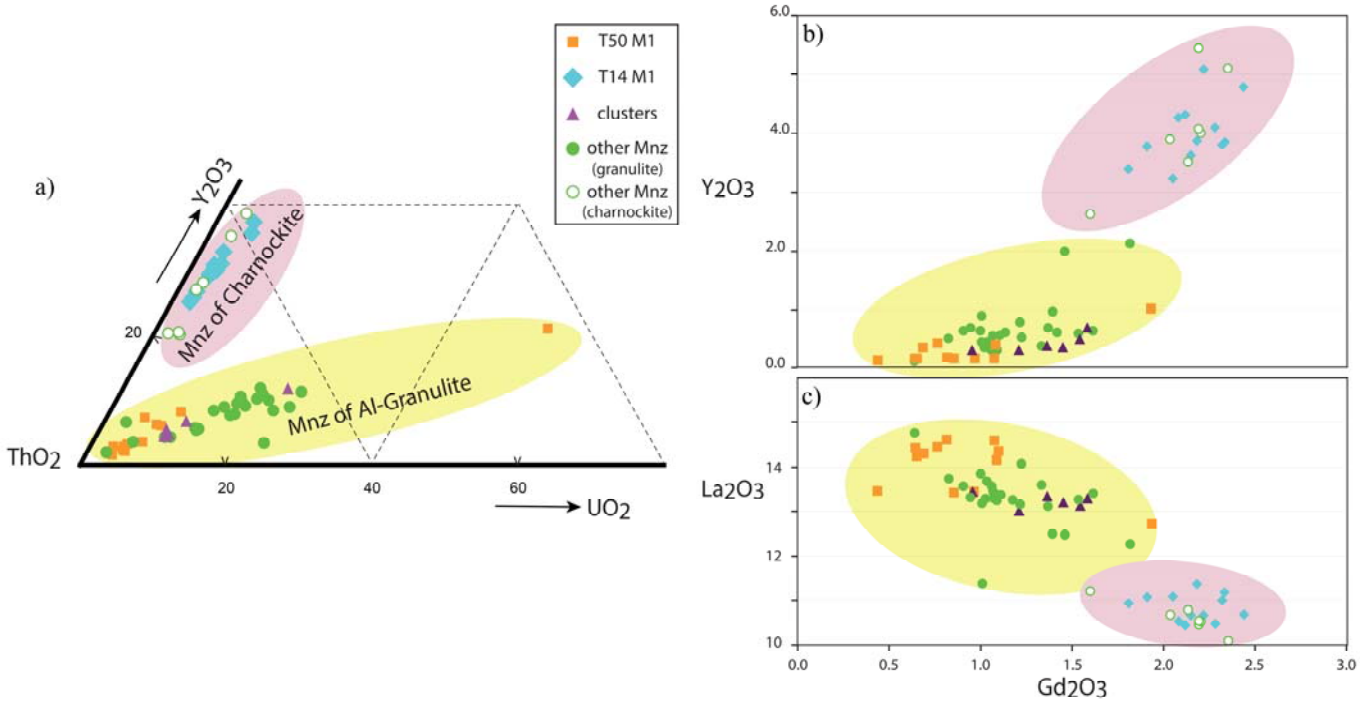

Figure 7

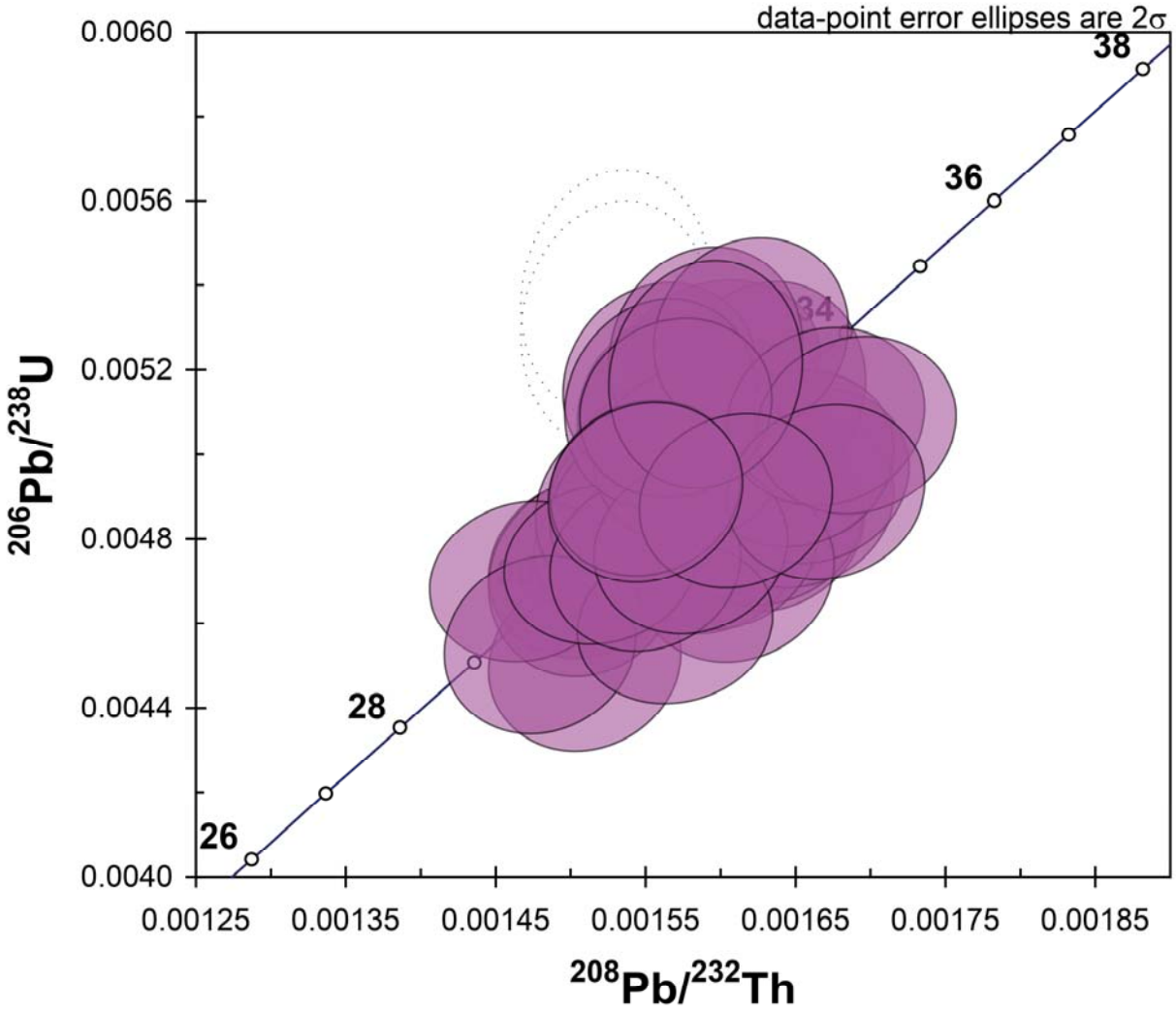

Figure 8 a

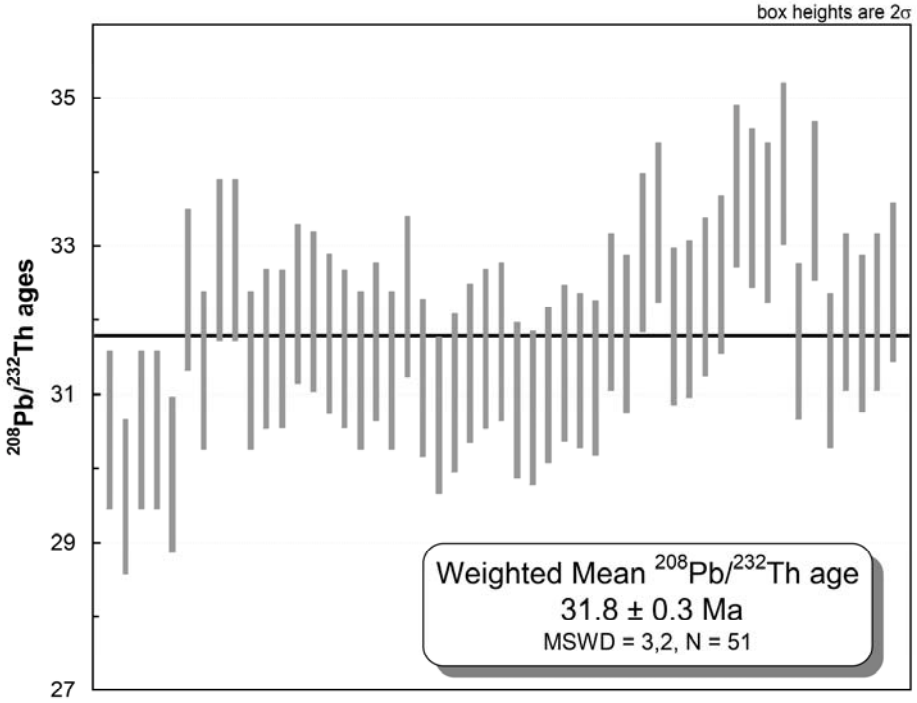

Figure 8 b

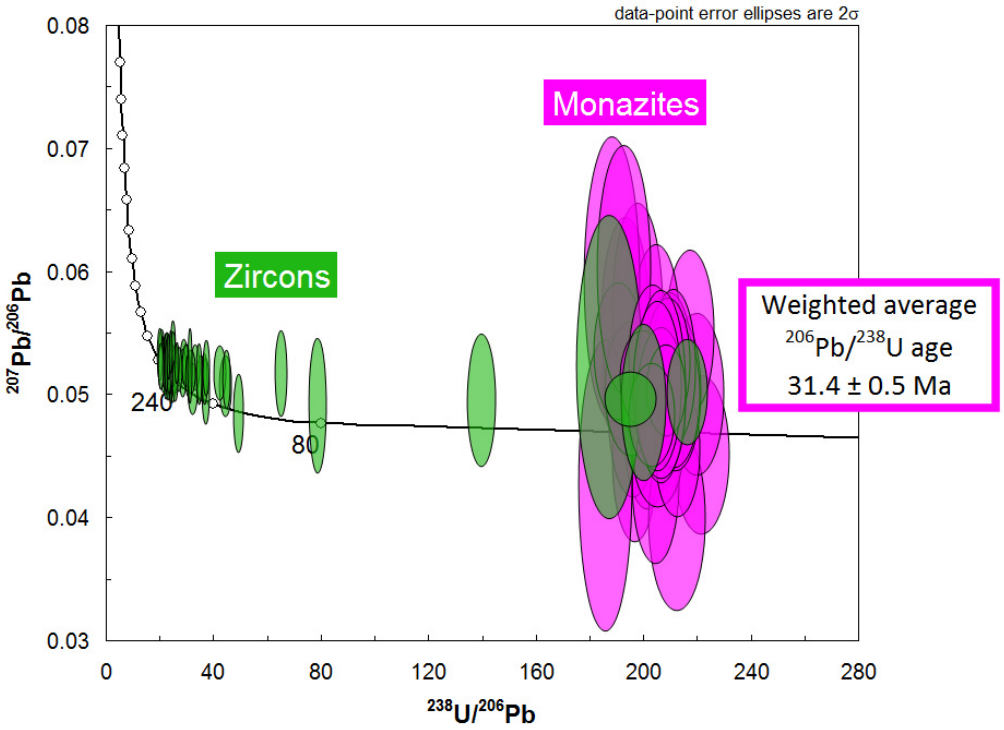

Figure 8c

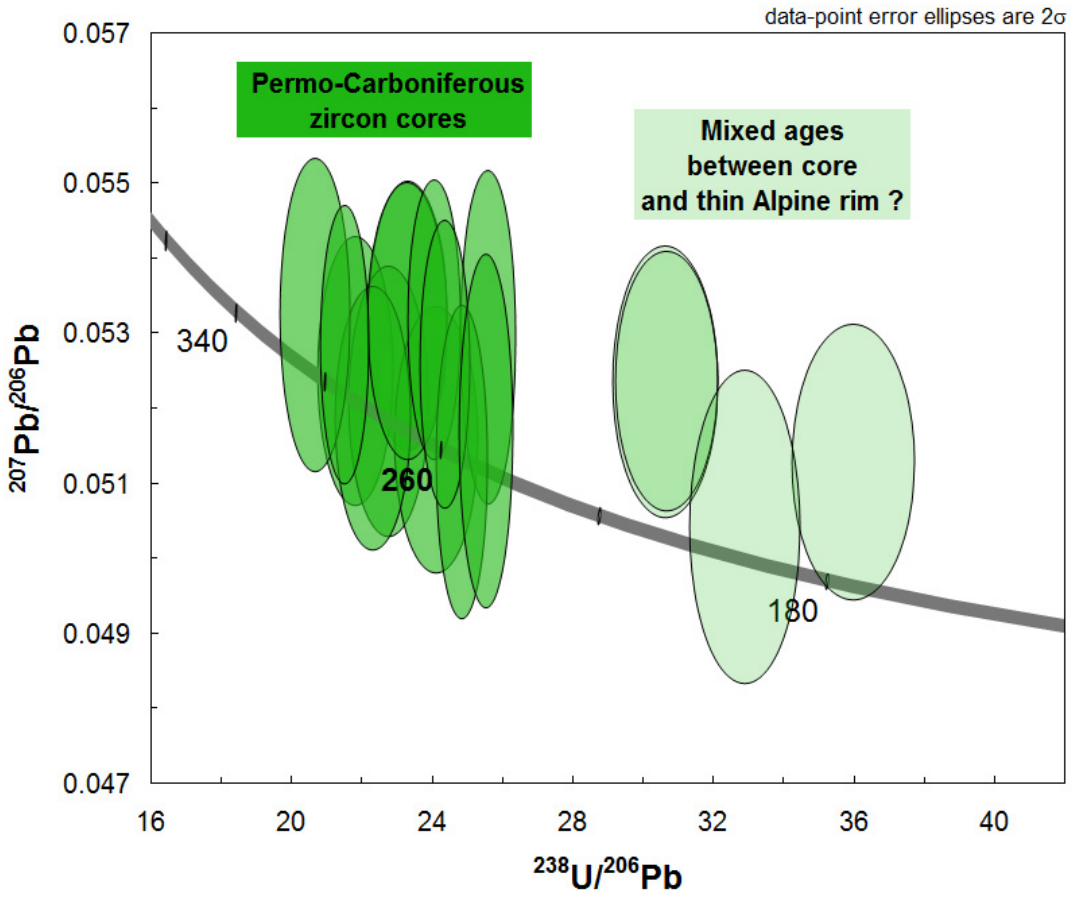

Figure 8 d